ASL-TR-0012

(12)

AD

Reports Control Symbol
OSD - 1366

THE EFFECT OF A SOLAR PROTON EVENT ON THE MINOR NEUTRAL CONSTITUENTS OF THE SUMMER POLAR MESOSPHERE

AUGUST 1978

By

MELVIN G. HEAPS

US Army Electronics Research and Development Command
Atmospheric Sciences Laboratory
White Sands Missile Range, NM 88002

NOTICES

Disclaimers

Disposition

REPORT DOCUMENTATION PAGE

READ INSTRUCTIONS
BEFORE COMPLETING FORM

1. REPORT NUMBER
ASL-TR-0012

2. GOVT ACCESSION NO.

3. RECIPIENT'S CATALOG NUMBER
⑨

4. TITLE (*and Subtitle*)
⑥ THE EFFECT OF A SOLAR PROTON EVENT ON THE MINOR NEUTRAL CONSTITUENTS OF THE SUMMER POLAR MESOSPHERE

5. ~~TYPE OF REPORT & PERIOD COVERED~~
Research and development
R&D Technical Report.

6. PERFORMING ORG. ~~REPORT NUMBER~~

7. AUTHOR(s)
⑩ Melvin G. Heaps

8. CONTRACT OR GRANT NUMBER(s)

9. PERFORMING ORGANIZATION NAME AND ADDRESS
Atmospheric Sciences Laboratory
White Sands Missile Range, New Mexico 88002

10. PROGRAM ELEMENT, PROJECT, TASK AREA & WORK UNIT NUMBERS
⑯
DA Task No. 1L162111AH71A4~~D2~~

11. CONTROLLING OFFICE NAME AND ADDRESS
US Army Electronics Research
and Development Command
Adelphi, MD 20783

12. REPORT DATE
⑪ August 1978 ⑰ A4

13. NUMBER OF PAGES
28

14. MONITORING AGENCY NAME & ADDRESS (*if different from Controlling Office*)
⑭ ERADCOM/ASL-TR-0012

15. SECURITY CLASS. (*of this report*)
UNCLASSIFIED

15a. DECLASSIFICATION/DOWNGRADING SCHEDULE

16. DISTRIBUTION STATEMENT (*of this Report*)
Approved for public release; distribution unlimited.
⑫ 33p.

17. DISTRIBUTION STATEMENT (*of the abstract entered in Block 20, if different from Report*)

18. SUPPLEMENTARY NOTES

19. KEY WORDS (*Continue on reverse side if necessary and identify by block number*)

D region	Ion chemistry
Mesosphere	Neutral chemistry
Solar proton event	HO_x O sub x
	NO_x

20. ABSTRACT (*Continue on reverse side if necessary and identify by block number*)

The increased ionization associated with a solar proton event serves as an additional source of NO_x and HO_x in the middle atmosphere. Detailed calculations show that upper limits of 1.3 NO_x and 1.8 HO_x per ion pair are applicable throughout most of the mesosphere. The enhanced number densities of ionized species affect the concentrations of several important minor neutral species, which in turn play an important role in the radiation and energy balance of the entire mesosphere. The increased → cont.

DD FORM 1 JAN 73 1473 EDITION OF 1 NOV 65 IS OBSOLETE

LB

410 663

20. ABSTRACT (cont)

ionization during the peak 24-hour period of the August 1972 SPE is capable of increasing the OH concentration and decreasing the O and O_3 concentrations up to an order of magnitude near 80 km, with smaller changes evident throughout the mesosphere. An exact determination of the immediate products of ionization events are necessary for correct assessment of Army nuclear weapons' effects (NWE) computer codes. Modeling a naturally occurring phenomenon such as solar proton event provides the opportunity to partially validate the sections of NWE codes which deal with post-burst effects in the middle atmosphere.

CONTENTS

INTRODUCTION

The measurements of mesospheric ozone by Weeks et al. [1] during the course of the November 1969 solar proton event showed an intriguing decrease in ozone. Other studies [2, 3] have indicated that such a decrease in mesospheric odd oxygen can be attributed to an increase in odd hydrogen due to enhanced ionization. The hydration of O_2^+ ions and the chain of reactions which leads to the hydronium ions $H_3O^+ \cdot (H_2O)_n$ produce an OH radical, and subsequent electron-ion recombination frees atomic hydrogen (see for example Reid [4]). These species of odd hydrogen, along with the concomitantly produced HO_2, serve as catalysts in an effective chain reaction which destroys odd oxygen in the mesosphere.

Various forms of odd nitrogen are also produced either directly during the actual ionization of air or rapidly thereafter via fast ion-molecule interactions. While catalytic destruction of odd oxygen by NO_x is important in the stratosphere, the destruction of odd oxygen is dominated by the HO_x chain reactions in the mesosphere.

In this study the time varying history of the particle induced ionization rates during the peak period of the August 1972 solar proton event is used to construct a detailed history of the odd hydrogen sources. A comparison is then made between the concentrations of H, OH, HO_2, O, and O_3 for the 4-5 August 1972 period of the solar proton event (SPE) and the same time period with the SPE sources removed. Attention is limited to the subsequent effects in the mesosphere.

The emphasis of this study is to determine the immediate products of ionization for later use as lumped parameters in large-scale nuclear weapons effects (NWE) simulation codes. Solar proton events, which produce large amounts of ionization in the middle atmosphere, are analogous to late-time effects of nuclear bursts. Successful modeling of such naturally occurring events serves to validate the sections of NWE codes which deal with post-burst effects in the middle atmosphere.

ION PRODUCTION RATES AND CHEMISTRY

The time dependent ion-pair production rate profiles are taken from Reagan and Watt [5] and Watt [6]. These profiles are shown in Fig. 1 for a few selected altitudes. The ionization profiles have been computed from satellite measurements of particle fluxes, but often these measurements are for widely divergent longitudes. The Chatanika radar showed a large enhancement of ionization mainly above 70 km, around 2200 UT on 4 August 1972 [5]; consequently, several points in Fig. 1 have been interpolated to match this feature. Since the satellite measurements have been made at varying longitudes, some uncertainty is introduced into the values when they are compiled for use at one location, particularly when auroral electrons make significant contributions.

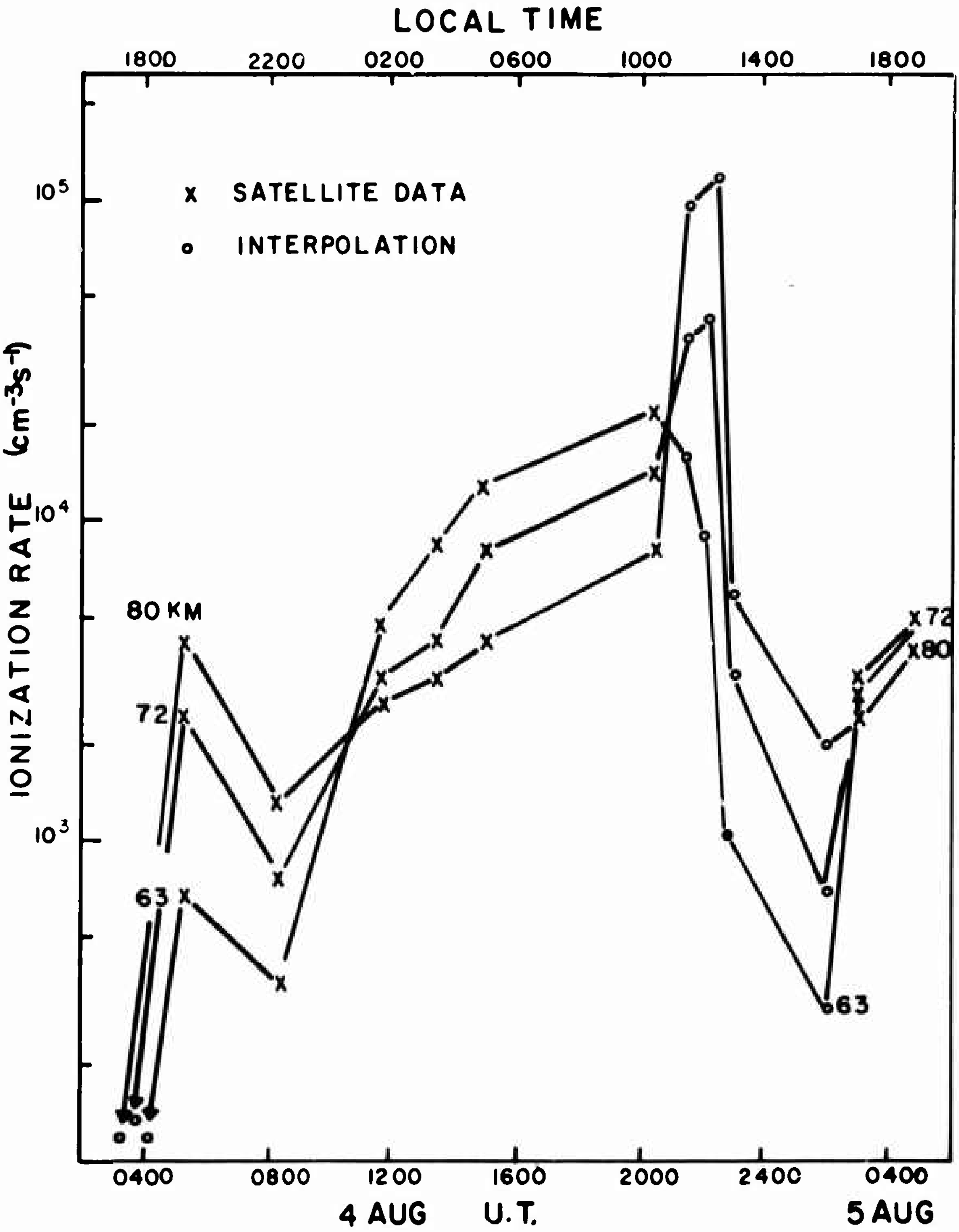

Figure 1. The time history of ionization rates during the August 1972 particle event at 80, 72, and 63 km.

In addition, the particle deposition profiles have been calculated for the CIRA 1965 mean reference atmosphere [7]. A comparison with a high latitude model for August (CIRA 1972 [8]) shows that these latter mesospheric densities are larger than those given in the mean reference atmosphere. Because of uncertainties in longitudinal correlation and auroral enhancements, the ion-pair production should be considered accurate only within approximately 20 percent (J. B. Reagan, private communication), which generally encompasses the uncertainties due to different model atmospheres. The ionization rates are therefore used as originally calculated, even though they may tend to somewhat underestimate actual values.

In the subsequent calculations dealing with the ion and neutral chemistries, the model atmosphere used for the major neutral constituents is the CIRA 1972, August 65° N model, with the corresponding temperature profile. The H_2O density is set at 5 ppm of the neutral number density. The initial densities of several minor neutral constituents are shown in Fig. 2. The boundaries of the 24-hour period under study, 03:06 UT 4 August to 03:06 UT 5 August, or 17:06 local time, have been chosen to match with available satellite data.

The neutral and ion chemistries are calculated by use of a large multispecies chemistry code called DIARCHEM (for D-region air chemistry) [9]. For the present study a configuration of 64 ion and neutral species and 493 reactions has been used which encompasses oxygen, nitrogen, hydrogen, and limited carbon chemistry. Suitable reviews of the neutral chemistry are available in the literature [10, 11]; the emphasis here will be on the ion-neutral chemistry.

The majority of odd nitrogen is produced directly during the ionization of N_2 by incident protons and (mainly) secondary electrons. Following the work of Porter et al. [12], the initial ratios are taken as 1.04 N atoms per ion pair (apportioned among the ^4S, ^2D, and ^2P states) and 0.154 N^+ atoms per ion pair. The baseline production of odd nitrogen may then be taken as 1.2 N atoms per ion pair, some of which are in excited and ionized states. These atoms are then converted to NO through rapid neutral reactions, ion-atom interchanges, and subsequent recombination. Roble and Rees [13] provide a good review of the two-body ion and neutral chemistries.

Additional odd nitrogen is formed by charge exchange and ion-atom interchanges by the other primary ions of the initial ionization occurrence. Table 1 lists the pertinent reactions which are involved in the formation of odd nitrogen after the initial ionization. At mesospheric heights, essentially all of the N_2^+ formed undergoes charge exchange with O_2 to form O_2^+, as does a majority of the O^+. About 20 to 25 percent of the O^+ undergoes an ion-atom interchange with N_2 to form NO^+ + N. Since

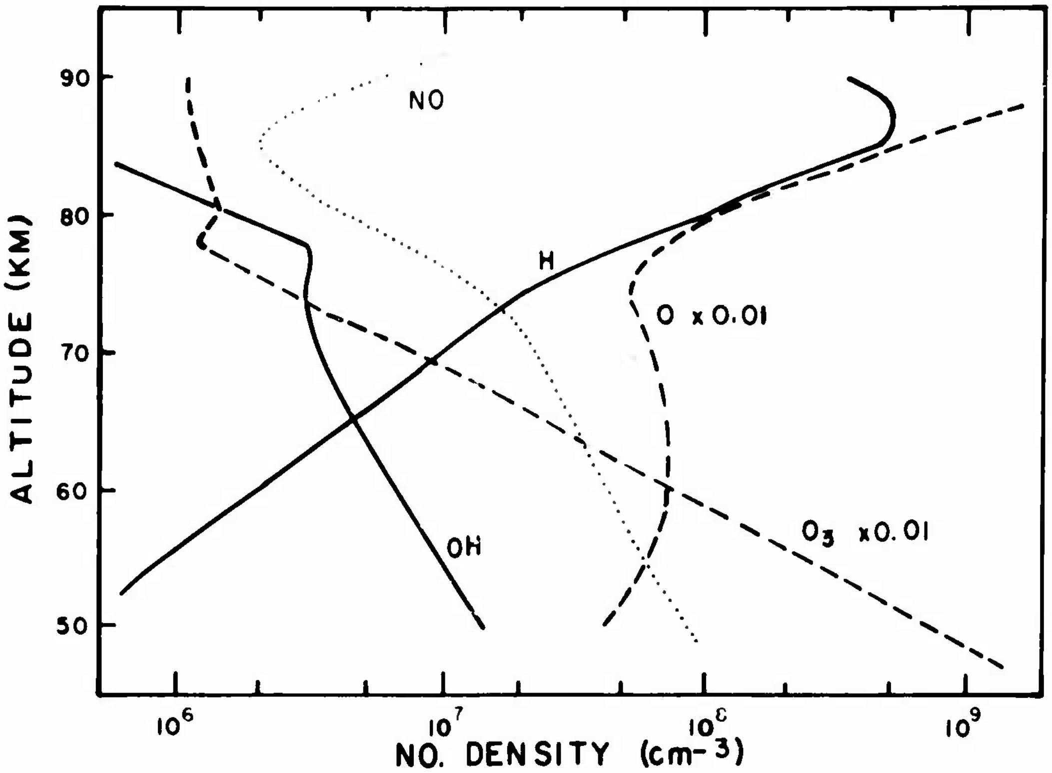

Figure 2. The densities of several minor neutral species at the beginning of the 24-hour period 03:06 UT 4 Aug (17:06 local time). Solar zenith angle is 69°.

TABLE 1. MAJOR ION-MOLECULE REACTIONS LEADING TO ODD NITROGEN

Reaction	Rate Constant
$N_2^+ + O_2 \rightarrow N_2 + O_2^+$	$5.0\ (-10)\ (300/T)^{0.8}$*
$O^+ + O_2 \rightarrow O + O_2^+$	$2.0\ (-11)\ (300/T)^{0.4}$
$O_2^+ + N_2 \rightarrow NO^+ + NO$	$<1.0\ (-15)$†
$O^+ + N_2 \rightarrow NO^+ + N$	$1.2\ (-12)\ (300/T)^{0.5}$
$O^+ + N_2 + M \rightarrow NO^+ + N + M$	$1.6\ (-29)\ (300/T)^{2.0}$

*Read as $5.0 \times 10^{-10}\ (300/T)^{0.8}\ cm^3 s^{-1}$, units of $cm^6 s^{-1}$ for three-body reactions.

†Reaction has never been observed; the rate constant, if the reaction proceeds, is below detection threshold.

there are 0.063 O^+ atoms formed per ion pair, the ratio of odd nitrogen formed per ion pair may be raised to 1.22.

In the stratosphere the three-body reaction $O^+ + N_2 + M \rightarrow N + NO^+ + M$ becomes important and below 40 km is most likely the dominant loss process for O^+, based on the four-fold increase in the apparent bimolecular rate of the three-body reaction over the same two-body reaction [14]. There may be a three-body charge transfer process $O^+ + O_2 + M \rightarrow O + O_2^+ + M$ which would continue to transfer the O^+ charge to O_2, but it has not been observed due to the fast rate for the two-body $O^+ + O_2$ charge exchange reaction. The potential $O^+ + O_2 + M$ reaction rate is probably the same order of magnitude as the measured $O^+ + N_2 + M$ rate (F. C. Fehsenfeld, private communication), so that the ion-atom interchange to form odd nitrogen is still the most likely loss process for O^+. Therefore, the odd nitrogen per ion pair ratio may well rise to 1.32 in the stratosphere.

The one other reaction which may produce odd nitrogen is $O_2^+ + N_2 \rightarrow NO^+ + NO$. The reaction rate is below measurement threshold and has been set at $< 10^{-15}$ cm^3s^{-1} [15]. For the purpose of this study, a value of 10^{-16} has been chosen. At this rate the $O_2^+ + N_2$ reaction is a negligible loss of O_2^+ in the stratosphere, but may become of some importance in the upper mesosphere under quiet to moderately disturbed conditions. Normally the major losses of O_2^+ in the mesosphere are recombination with electrons, charge transfer with NO, and processes leading to hydration. In the upper mesosphere the lifetime of O_2^+ is long enough that a fraction of the O_2^+ may undergo the ion-atom interchange with N_2. This fraction decreases with increasing ionization levels so that in the mesosphere the odd nitrogen production ratio will exceed 1.22, but will fall back toward this figure as the level of ionization increases.

In summary, the lower bound for the odd nitrogen per ion pair ratio is 1.22, but may be somewhat higher in the upper mesosphere due to the unmeasured $O_2^+ + N_2$ reaction. In the stratosphere the ratio may increase to 1.32, which can reasonably serve as an upper limit throughout the entire middle atmosphere.

The eventual formation of odd hydrogen from the initial ionization occurrence follows a less direct and correspondingly somewhat slower route than that of odd nitrogen. The primary ion-neutral and ion-recombination reactions which lead to the production of odd hydrogen and the subsequent neutral reactions which destroy odd oxygen are listed in Table 2.

TABLE 2. SELECTED REACTIONS AND THEIR RATE CONSTANTS LEADING TO ODD HYDROGEN

a.	$O_2^+ + O_2 + M \rightarrow O_4^+ + M$	$3.9\ (-30)\ (300/T)^{3.2*}$
b.	$O_4^+ + H_2O \rightarrow O_2^+\cdot H_2O + O_2$	$1.5\ (-9)$
c.	$O_2^+\cdot H_2O + H_2O \rightarrow H_3O^+\cdot OH + O_2$	$1.0\ (-9)$
d.	$O_2^+\cdot H_2O + H_2O \rightarrow H_3O^+ + OH + O_2$	$2.0\ (-10)$
e.	$H_3O^+\cdot OH + H_2O \rightarrow H_3O^+\cdot H_2O + OH$	$1.4\ (-9)$
f.	$H_3O^+ + N_2 + M \rightarrow H_3O^+\cdot N_2 + M$	$1.4\ (-30)\ (300/T)^{4.0}$
g.	$H_3O^+\cdot N_2 + H_2O \rightarrow H_3O^+\cdot H_2O + N_2$	$1.0\ (-9)$
h.	$H_3O^+\cdot OH(\mathrm{or}\ N_2) + e \rightarrow H + OH(\mathrm{or}\ N_2) + H_2O$	$2.0\ (-6)\ (300/T)^{0.2}$
i.	$H_3O^+\cdot (H_2O)_n + e \rightarrow H + (n+1)\cdot H_2O$	$1.3 - 7.4\ (-6)\ (300/T)^{0.2}$
j.	$H_3O^+\cdot (H_2O)_n$- $+ X^- \rightarrow$ products	$6.0\ (-8)$
k.	$H_3O^+\cdot H_2O + H_2O + M \rightarrow H_3O^+\cdot (H_2O)_2 + M$	$2.3\ (-27)\ (300/T)^{4.0}$
l.	$NO^+\cdot (H_2O)_3 + H_2O \rightarrow H_3O^+\cdot (H_2O)_2 + HNO_2$	$7.0\ (-11)$
m.	$H_3O^+(H_2O)_n + H_2O + M \rightarrow H_3O^+\cdot (H_2O)_{n+1} + M$	$2.4 - 0.9\ (-27)\ (300/T)^{4.0}$
n.	$O + OH \rightarrow H + O_2$	$4.2\ (-11)$
o.	$H + O_3 \rightarrow OH + O_2$	$1.2\ (-10)\ \exp\ (-562/T)$
p.	$H + O_2 + M \rightarrow HO_2 + M$	$2.1\ (-32)\ \exp\ (+290/T)$
q.	$HO_2 + O \rightarrow OH + O_2$	$3.0\ (-11)$

*Read as $3.9 \times 10^{-30}(300/T)^{3.2}$; units in cm^3s^{-1} for two-body reactions, cm^6s^{-1} for three-body reactions.

Figures 3a and 3b illustrate the flow of ion reactions which produce odd hydrogen and the flow of neutral reactions which consume odd oxygen. Only the major paths have been shown; and although many ion reactions have appreciable reverse rates [16], only the forward directions are illustrated. However, the alternate paths and reverse rates have been included in the detailed calculations. The values for the production rates at noon (local time) for the SPE and quiet day cases at 80 km are given in Table 3. In each case these values represent maxima in ion-pair production and are the net values in the direction indicated.

RESULTS

Table 3 shows that a solar proton event results in a tremendous flow of charge through the positive ion chain, with the main channel being the two-step hydration of O_2^+ to $H_3O^+\cdot OH$, subsequent hydrations to $H_3O^+\cdot H_2O$, and then ion-electron recombination. Reaction paths 18 and 19 in Fig. 3b, which sum the effects of all hydration and recombination reactions producing odd hydrogen, show that the SPE induced production of H and OH can exceed the normal sunlight production through dissociation of H_2O by more than a factor of 20.

Figure 4 shows the altitude profiles of the SPE induced H and OH production rates as well as the normal sources due to the dissociation of water by sunlight and $O(^1D)$. Also shown are the electron and summed hydronium ion densities. The hydration and recombination of the SPE induced ionization are obviously the dominant sources throughout most of the mesosphere. These sources of H and OH are controlled by the rather sharp $H_3O^+\cdot(H_2O)_n$ ledge at 82 km, by the decreasing effect of electron-ion recombination due to decreasing electron density, and finally by the increasing importance of ion-ion recombination, which potentially serves as an additional source of OH, as one nears the stratopause.

The effect of the increased production of odd hydrogen on the odd oxygen densities can best be illustrated by plotting the ratio of the disturbed day SPE densities to the quiet day densities as is done in Fig. 5. The relative effect is greatest near 80 km, which correlates with the maximum in odd hydrogen production shown in Fig. 4. Normally the greatest loss process for atomic oxygen is its recombination with O_2 to form ozone. The greatly increased production of odd hydrogen causes a large drop in atomic oxygen density due to the reactions $O + OH$ and $O + HO_2$ becoming the larger loss processes above 65 km. The reduced atomic oxygen results in a lowered ozone density because of the decrease in the recombination of O with O_2. Loss of ozone through odd hydrogen reactions is secondary to photodestruction processes. Therefore the relative changes in the ozone profile are closely coupled to those in the atomic oxygen profile, as is illustrated in Fig. 5. Likewise, the speed of the reaction $H + O_2 + M$ in converting H to HO_2 is sufficient to insure that

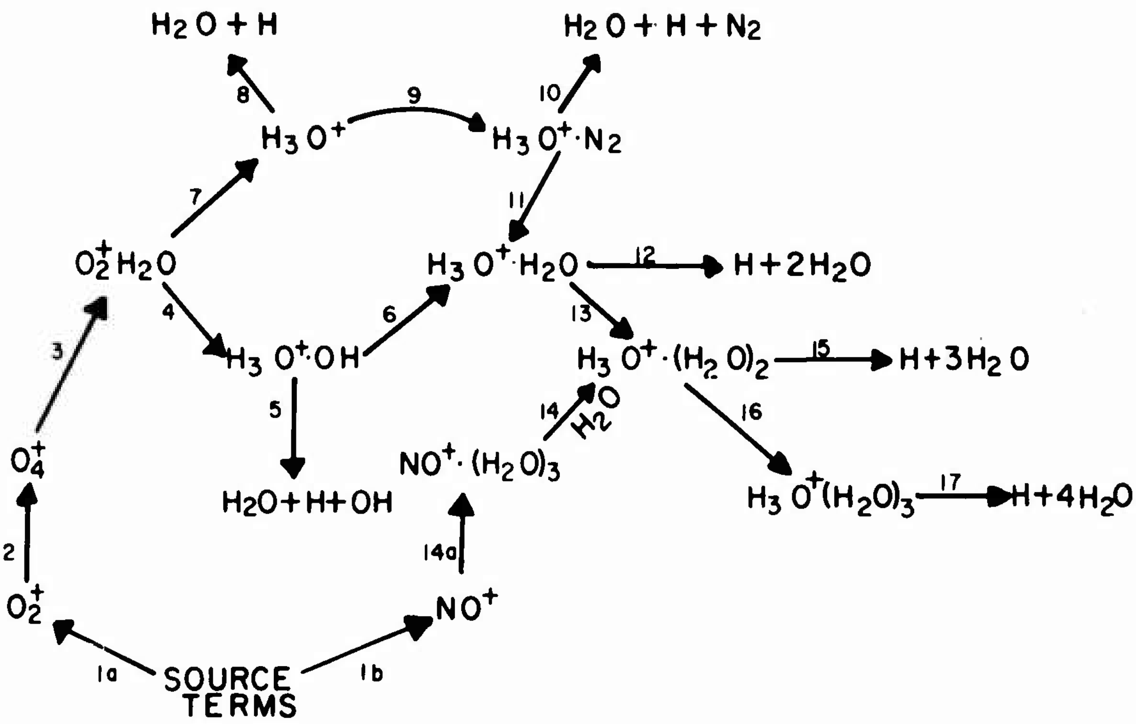

Figure 3a. The reaction paths in the positive ion chain. Odd hydrogen is produced at steps 4 to 8, 10, 12, 15, and 17. The production rates at 80 km, local noon, are given in Table 3 for each of the steps.

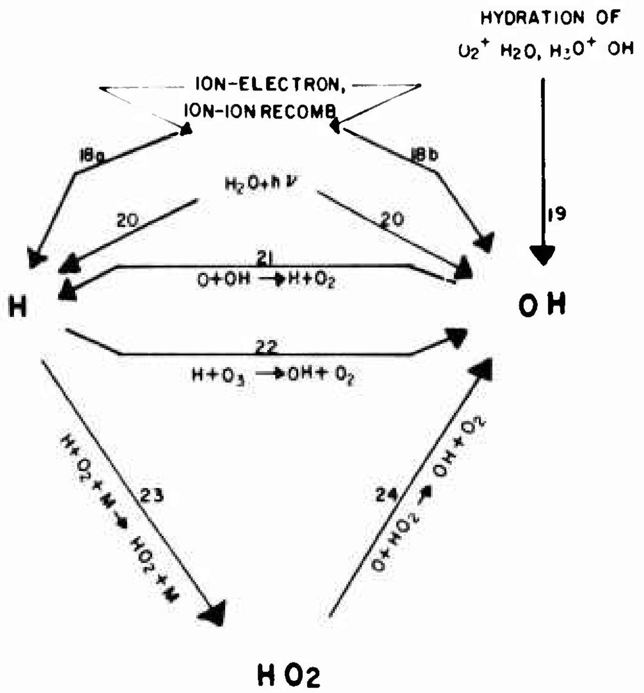

Figure 3b. The reaction paths in the positive ion, neutral chain. Nascent odd hydrogen is introduced at steps 18 to 20. The production rates at 80 km, local noon, are given in Table 3 for each of the steps.

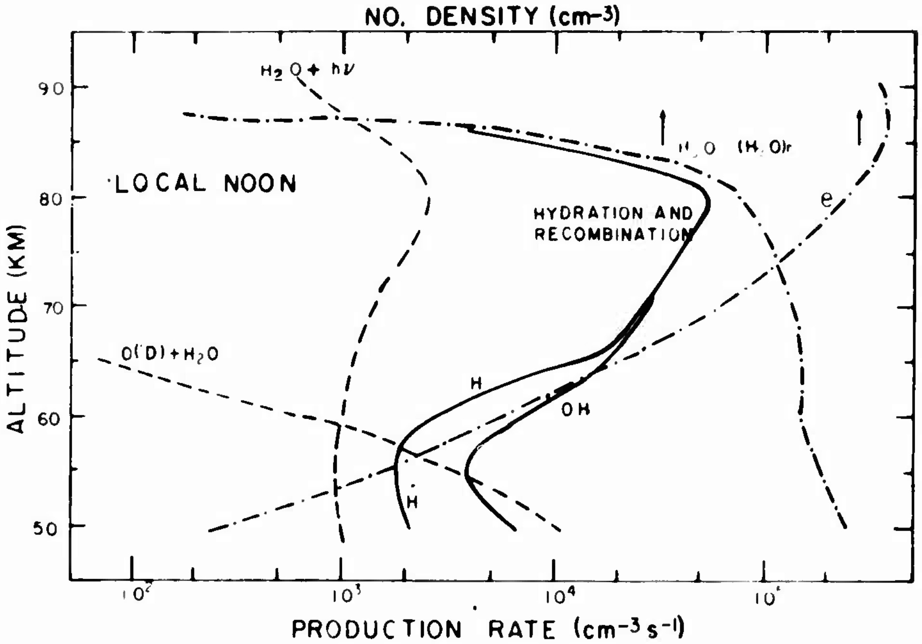

Figure 4. The electron and total hydronium ion densities (dotted lines) at local noon during the August 1972 SPE. Also shown are the H and OH production rates due to photodissociation of water, hydration, and recombination of ions, and action of $O(^1D)$ on water.

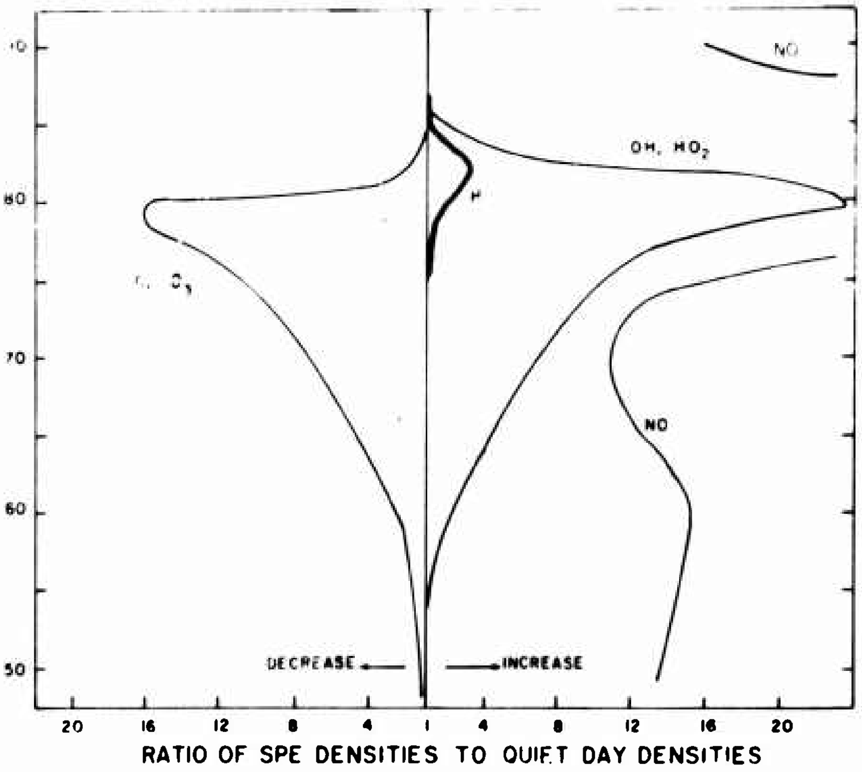

Figure 5. The ratio of the SPE disturbed day densities of O, H. OH, and NO to those for the corresponding quiet day. The ratios for the O_3 and HO_2 densities are very similar to the O and OH ratios, respectively.

TABLE 3. PRODUCTION RATE VALUES

Path (Figs. 3a + b)	Reaction Table 2	Production Rates at 80 km ($cm^{-3}s^{-1}$)	
		SPE	Quiet Day
1a	(see Fig. 1)	1.0 (5)*	1.7 (-2)
1b		1.9 (4)	9.1 (-1)
2	a	8.6 (4)	1.7 (-2)
3	b	6.5 (4)	1.7 (-2)
4	c	4.7 (4)	1.3 (-2)
5	h	6.9 (3)	<1. (-4)
6	e	4.0 (4)	1.3 (-2)
7	d	9.4 (3)	2.6 (-3)
8	i	1.0 (3)	<1. (-4)
9	f	8.4 (3)	3.5 (-1)**
10	h	1.3 (3)	<1. (-4)
11	g	7.1 (3)	3.5 (-1)
12	i,j	4.5 (4)	1.2 (-2)
13	k	1.7 (3)	3.5 (-1)
14a	(see Reid, 1977)	3.2 (1)	5.3 (-1)
14b	l	5.3 (0)	5.2 (-1)
15	i,j	1.7 (3)	5.1 (-2)
16	m	3.6 (1)	8.2 (-1)
17	i,j	3.6 (1)	8.2 (-1)
18a	i,j	5.6 (4)	8.9 (-1)
18b	i,j	6.9 (3)	<1. (-4)
19	c,d	4.9 (4)	1.6 (-2)
20	(see Fig. 4)	2.5 (3)	2.7 (3)
21	n	1.2 (6)	6.9 (5)
22	o	1.2 (4)	7.6 (4)
23	p	1.2 (6)	6.1 (5)
24	q	1.1 (6)	6.1 (5)

*Read as 1.0×10^5 $cm^{-3}s^{-1}$

**The increase in this production rate is due to another source of H_3O^+ via the reaction $NO^+\cdot(H_2O)_2 + h\nu \rightarrow H_3O^+ + HNO_2$ to which a tentative cross section of $\lesssim 3 \times 10^{-20}$ cm^2 has been assigned.

most of the odd hydrogen created below 80 km resides as HO_2 and OH, while the similar rates of reactions 21 and 24 insure that relative changes in the HO_2 and OH profiles are closely coupled. Only above 78 km does the three-body conversion of H to HO_2 begin to slow sufficiently to allow a buildup in the H concentration, but even this increase is limited by the rapid decrease in the SPE sources of odd hydrogen above 82 km shown in Fig. 4.

The number of H atoms and OH molecules produced per ion pair is a useful quantity and one which is readily derivable when the detailed chemistry is considered. The upper limit is nominally two odd hydrogens per ion pair, one OH being produced during the hydration of O_2^+ and an H atom being liberated during subsequent recombination of $H_3O^+ \cdot (H_2O)_n$. In practice the recombination and charge-exchange of the precursor ions yield a value less than two. Figure 6 shows the ratio of (H + OH) and odd nitrogen per ion pair for two values of the ion-pair production rate. For altitudes above 70 km, the higher ion-pair production rate yields a noticeably smaller ratio of (H + OH), due mainly to the more rapid rate of ion-electron recombination for precursor ions. Even below 70 km, the ratio remains slightly lower for higher production rates because of increased charge exchange with enhanced NO concentrations found under more disturbed conditions. The net result is that the odd hydrogen production ratio has an effective upper limit of about 1.8 per ion pair below 80 km with appreciably lower values possible as the ion-pair production rate increases. The relative proportion of OH to H increases below 60 km, as can be seen in Fig. 4, due to recombination of $H_3O^+ \cdot (H_2O)_n$ with the more prevalent negative ions CO_3^- and NO_3^-, which is felt to yield an OH radical rather than separate H and O atoms.

DETAILED VARIATIONS IN TIME

The detailed time history of the odd oxygen and odd hydrogen species during the 4-5 August SPE maximum can best be understood if the normal quiet day variations are first examined. The time history of the densities at 80 km for the 24-hour period under study are shown in Fig. 7. The atomic oxygen density, under solar control to a great degree, is rapidly decreasing because of the growing attenuation of the solar flux shorter than 250 nm. By 17:00 local time, the loss processes O + HO_2 and O + OH, shown as reaction paths 23 and 24 in the odd hydrogen catalytic cycle in Fig. 3b, have become the dominant losses for atomic oxygen, exceeding even the O + O_2 + M recombination mechanism. The ozone profile closely follows the atomic oxygen profile (they are essentially in photochemical equilibrium) until the solar flux <310 nm is absorbed at a solar zenith angle > 91 degrees. At this point the ozone density briefly, but rapidly, increases at the expense of atomic oxygen until the still declining atomic oxygen density can no longer support such

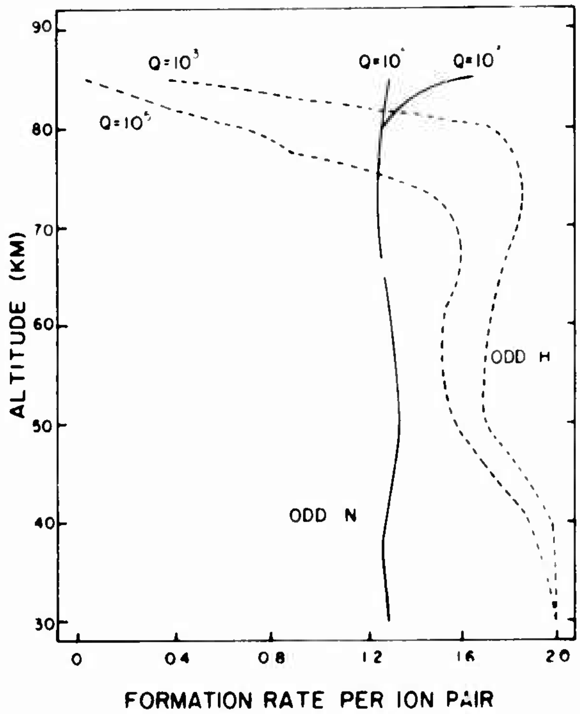

Figure 6. The ratio of (H + OH) and odd nitrogen production per ion pair for high and low values of the ion-pair production rate Q.

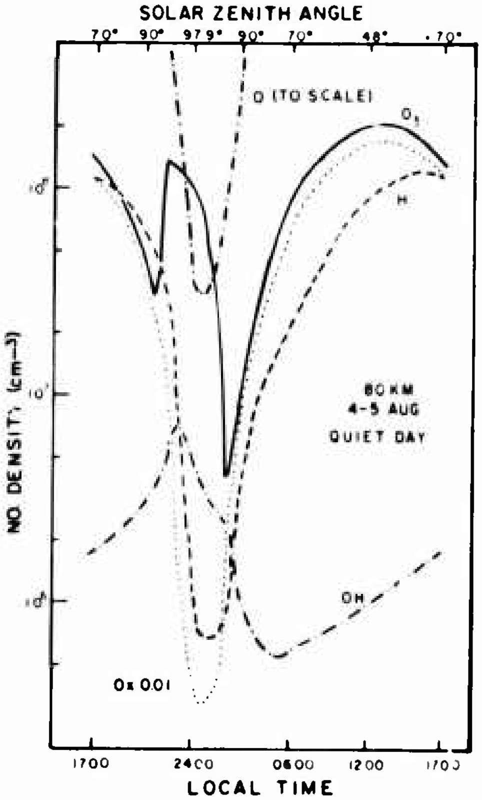

Figure 7. The O, O_3, OH, and H density time-profiles at 80 km for the simulated quiet day densities during 4-5 August. Note that the O density profile is shown twice, once to scale and again multiplied by a factor of 0.01.

growth. This fluctuation in ozone is accentuated by the "slow" sunset due to the high latitude, summer conditions. (At 80 km the sun does not dip below the horizon at this time of year, although the solar UV flux is absent for approximately 3 hours about local midnight.) Ozone is dissociated by visible light at all times, which accounts for its decay during the midnight period.

The initial source of atomic hydrogen is the photodissociation of water vapor, though the total density is essentially controlled by the $O + OH \rightarrow H + O_2$ reaction in the odd hydrogen cycle. Consequently, the atomic hydrogen density profile closely follows that of atomic oxygen. The afternoon decrease in atomic oxygen also causes an increase in the OH concentration because the same $O + OH$ reaction is the dominant loss process for OH. The abundance of H relative to OH (and HO_2) insures that there is sufficient flow along the $H + O_2 + M$ and $HO_2 + M$ paths to keep the OH density increasing until it is larger than the rapidly declining H density. The sharpness of the peak in the OH density is due to the twilight increase in O_3 and the increased relative importance of the $H + O_3 \rightarrow OH + O_2$ reaction.

The continuing decrease in atomic oxygen carries through until shortly after midnight because of the dominance of the odd hydrogen losses. The first increase in atomic oxygen comes from the continuing visible photodissociation of ozone followed by a much steeper increase about an hour later due to the returning dissociation of O_2. The ozone density does not begin to increase until the atomic oxygen density has built up enough to reestablish photochemical equilibrium. Throughout the late afternoon until past midnight, the total odd hydrogen is decreasing because the reactions among the species of odd hydrogen themselves, forming mainly H_2O, are proceeding faster than the photodissociation of water vapor. Shortly past midnight, the increasing atomic oxygen density begins to build up the H density, principally at the expense of OH (and HO_2), through reaction path 21, $O + OH \rightarrow H + O_2$. Subsequent increase of the atomic hydrogen density and the eventual growth of the OH density beginning in the early morning are now due to the increasing photodissociation of water vapor into H and OH. The large amounts of atomic oxygen present during the day insure that most of the "new" H and OH produced are eventually stored as H.

In summary, for the quiet-day situation, atomic oxygen exhibits a large degree of solar control and is the dominant minor neutral species. Ozone is entirely controlled by atomic oxygen and direct solar influence. OH and HO_2 serve as the major loss processes for atomic oxygen in the late afternoon through midnight period, with decreasing O concentrations leading to increasing OH and HO_2 concentrations in a positive feedback mechanism. The H density serves essentially as a reservoir of odd hydrogen and closely follows the O density time profile, thus limiting the positive feedback between O and OH.

The disturbed time density profiles follow a pattern similar to the quiet-day profiles and it is more instructive to examine the ratio of disturbed-day densities to quiet-day densities for the 4-5 August period as shown in Fig. 8. The relative rise in OH (with most of the odd hydrogen being stored in the atomic hydrogen reservoir) causes a decline in the O density and, consequently, the O_3 density. Falling odd oxygen densities and secondarily a declining ion-pair production rate then cause the H reservoir to begin to empty and a corresponding rapid rise in the relative OH density. Rapidly declining H densities cause the ratio of the OH densities to begin decreasing about an hour later. The net effect is that the enhanced odd hydrogen production causes initial drop in odd oxygen with the result that the relative amount of atomic hydrogen during the nighttime period is lower; i.e., the daytime reservoir of atomic hydrogen is more completely drained. During the midnight period, the relative ratio of atomic oxygen actually increases because the particle induced dissociation of O_2 exceeds the solar photon induced dissociation [17]; this effect is enhanced by the increasing ion-pair production rate during this late night period. The relative concentrations of H and in turn OH and HO_2 begin to rapidly increase again. The increase in odd hydrogen gradually halts the relative increase in odd oxygen; the growing depletion of atomic oxygen causes the relative rate of increase in odd hydrogen to decline (note, however, that the total amount of odd hydrogen is increasing).

The sudden peak in the ion-pair production rate at local noon serves as perhaps the clearest example of what enhanced ionization can do. The response time of the H density (i.e., that time it would take to replace the H density from the SPE generated odd hydrogen) is $\sim$ 2000 s, that of OH $\sim$ 400 s, at this peak period. Lifetimes against being transformed by reaction paths 21 and 23 (Fig. 3b) are about 20 s for OH and 140 s for H. The response of the odd hydrogen densities to the changing SPE source is therefore limited by the H response time, and most of the odd hydrogen is initially stored as H. The lifetime of O against destruction by OH and HO_2 is $\sim$ 500 s during these disturbed conditions (as opposed to $\sim$ 13,000 s for a quiet day noon); therefore, the O density begins to decrease as rapidly as the OH and HO_2 densities increase - at essentially the H atom density response time. During the peak of the ion pair production, the lifetime of odd hydrogen species (principally H) against recombination to even hydrogen species (principally H_2O) is $\sim$ 4000 s, much longer than the drop-off time associated with this particular ionization peak. The increase in odd oxygen is governed by the solar photon dissociation of O_2 which has a time constant of $\gtrsim$ 400 s near noon for these reduced odd oxygen densities. The main loss of odd oxygen is to the odd hydrogen, and odd hydrogen decays with the above stated lifetime of $\sim$ 400 s.

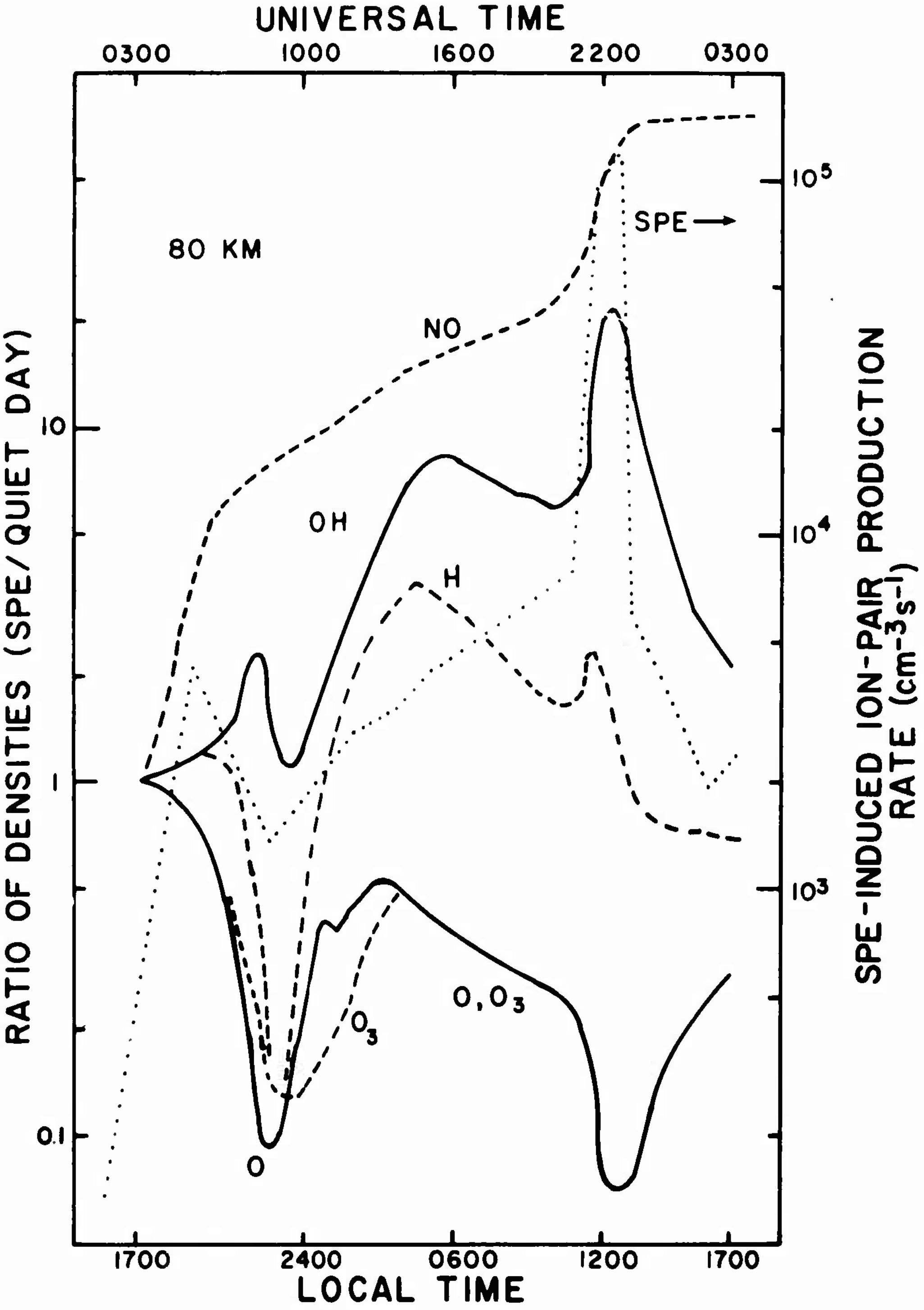

Figure 8. The ratio of the disturbed day (SPE) densities to the quiet day densities for the 4-5 August 1972 time period. Also shown is the SPE induced ion-pair production rate for the same 24-hour period.

To summarize, the density of odd hydrogen species can respond to changes in the ion-pair production rate on time scales of less than an hour near 80 km. In the upper mesosphere the odd hydrogen produced is mainly stored as H. In the lower mesosphere OH and HO_2 gradually becomes the reservoir for odd hydrogen. The decay time for odd hydrogen is somewhat more than an hour near 80 km. The odd oxygen is principally under solar control for its production, but its major loss processes during disturbed conditions are with odd hydrogen, and therefore changes in odd oxygen densities generally follow the time scales of the odd hydrogen. In sunrise/sunset situations, the rapidly changing solar influence may dominate particle precipitation effects or, as is more likely, make it difficult to clearly separate the two effects.

CONCLUSIONS

The greatly enhanced number densities of ionized species during a solar proton event affect the concentrations of several of the important minor neutral species in the mesosphere. The change is brought about through the enhanced production of odd hydrogen and odd nitrogen in the positive ion chain. A practical upper limit for (H + OH) production per ion pair below 80 km is 1.8. This ratio rapidly decreases above 80 km, more so for increased ionization rates. The odd nitrogen production ratio varies within the narrower limits of 1.2 to 1.3. Within the mesosphere, the production of odd hydrogen drives the changes in the minor neutral constituent chemistry.

The increased ionization during the peak 24-hour period of the August 1972 SPE is capable of increasing the OH concentration and decreasing the O and O_3 concentrations up to a factor of 20 near 80 km, with smaller changes apparent throughout the mesosphere.

The time constants associated with the creation of odd nitrogen, and the resultant increase in the NO concentration, are rapid enough (< 1 s) to be considered simultaneous with the ionization event. However, the removal of NO in the mesosphere is very slow so that enhanced NO concentrations persist for days, finally to be altered by large-scale transport phenomena. The time constants associated with increases in odd hydrogen, and consequently with decreases in odd oxygen, are $\gtrsim 2 \times 10^3$ s, while removal times of odd hydrogen in the mesosphere are $\gtrsim 4 \times 10^3$ s. Thus the response of the oxygen-hydrogen chemistries and densities to an ionizing event is on the time scale of a few hours, while the return to photochemical equilibrium is on the time scale of several hours to a few days.

It is important to be able to determine the immediate products and effects of enhanced ionization in the atmosphere so that they may be used as lumped parameters in large-scale NWE simulation codes. Solar proton events produce ionization effects which are analogous to late-time effects of nuclear bursts. Successful modeling of such naturally occurring events serves to validate the sections of NWE codes which deal with post-burst effects in the middle atmosphere.

REFERENCES

1. Weeks, L. H., R. S. Cuikay, and J. R. Corbin, 1972, "Ozone Measurements in the Mesosphere During the Solar Proton Event of 2 November 1969," J. Atmos. Sci., 29:1138-1142.

2. Swider, W., and T. J. Keneshea, 1973, "Decrease of Ozone and Atomic Oxygen in the Lower Mesosphere During a PCA Event," Planet. Space Sci., 21:1969-1973.

3. Frederick, J. E., 1976, "Solar Corpuscular Emission and Neutral Chemistry in the Earth's Middle Atmosphere," J. Geophys. Res., 81:3179-3186.

4. Reid, G. C., 1976, "Ion Chemistry in the D Region," Adv. Atomic and Molec. Phys., 12:375-413, Academic Press.

5. Reagan, J. B., and T. M. Watt, 1976, "Simultaneous Satellite and Radar Studies of the D Region Ionosphere During the Intense Solar Particle Event of August 1972," J. Geophys. Res., 81:4579-4596.

6. Watt, T. M., 15 July 1975, "Effective Recombination Coefficients of the Polar D Region Under Conditions of Intense Ionizing Radiation," Stanford Research Institute Defense Nuclear Agency Topical Report, DNA 3663T.

7. Gunton, R. C., R. E. Meyerott, and J. B. Reagan, 1977, "Ion and Neutral Chemistry of the D Region During the Intense Solar Particle Event of 1972," Lockheed Final Report, LMSC-D556351.

8. CIRA 1972, COSPAR International Reference Atmosphere 1972, Akademieverlag, Berlin, 1972.

9. Hoock, D. W., and M. G. Heaps, 1978, "DAIRCHEM: A Computer Code to Model Ionization-Deionization Processes and Chemistry in the Middle Atmosphere," ASL Internal Report, Atmospheric Sciences Laboratory, US Army Electronics Research and Development Command, WSMR, NM 88002.

10. Crutzen, P. J., 1974, "A Review of Upper Atmospheric Photo-Chemistry," Can. J. Chem., 52:1569-1581.

11. Nicolet, M., 1974, "An Overview of Aeronomic Processes in the Stratosphere and Mesosphere," Can. J. Chem., 52:1381-1396.

12. Porter, H. S., C. H. Jackman, and A. E. S. Green, 1976, "Efficiencies for Production of Atomic Nitrogen and Oxygen in Relativistic Proton Impact in Air," J. Chem. Phys., 65:54-167.

13. Roble, R. G., and M. H. Rees, 1977, "Time Dependent Studies of the Aurora," Planet. Space Sci., 25:991-1010.

14. Bohme, D. K., D. B. Dunkin, F. C. Fehsenfeld, and E. E. Ferguson, 1969, "Flowing Afterglow Studies of Ion-Molecule Association Reactions," *J. Chem. Phys.*, 51:863-872.

15. Ferguson, E. E., 1974, "Laboratory Measurements of Ionospheric Ion-Molecule Reaction Rates," *Rev. Geophys. Space Phys.*, 12:703-713.

16. Reid, G. C., 1977, "The Production of Water-Cluster Positive Ions in the Quiet Daytime D Region," *Planet. Space Sci.*, 25:275-290.

17. Heaps, M. G., 1976, "Minor Constituent Chemistry During a Solar Proton Event, EOS," *Trans. Amer. Geophys.*, U., 57:972.

DISTRIBUTION LIST

Dr. Frank D. Eaton
Geophysical Institute
University of Alaska
Fairbanks, AK 99701

Commander
US Army Aviation Center
ATTN: ATZQ-D-MA
Fort Rucker, AL 36362

Chief, Atmospheric Sciences Div
Code ES-81
NASA
Marshall Space Flight Center,
AL 35812

Commander
US Army Missile R&D Command
ATTN: DRDMI-CGA (B. W. Fowler)
Redstone Arsenal, AL 35809

Redstone Scientific Information Center
ATTN: DRDMI-TBD
US Army Missile R&D Command
Redstone Arsenal, AL 35809

Commander
US Army Missile R&D Command
ATTN: DRDMI-TEM (R. Haraway)
Redstone Arsenal, AL 35809

Commander
US Army Missile R&D Command
ATTN: DRDMI-TRA (Dr. Essenwanger)
Redstone Arsenal, AL 35809

Commander
HQ, Fort Huachuca
ATTN: Tech Ref Div
Fort Huachuca, AZ 85613

Commander
US Army Intelligence Center & School
ATTN: ATSI-CD-MD
Fort Huachuca, AZ 85613

Commander
US Army Yuma Proving Ground
ATTN: Technical Library
Bldg 2100
Yuma, AZ 85364

Naval Weapons Center (Code 3173)
ATTN: Dr. A. Shlanta
China Lake, CA 93555

Sylvania Elec Sys Western Div
ATTN: Technical Reports Library
PO Box 205
Mountain View, CA 94040

Geophysics Officer
PMTC Code 3250
Pacific Missile Test Center
Point Mugu, CA 93042

Commander
Naval Ocean Systems Center (Code 4473)
ATTN: Technical Library
San Diego, CA 92152

Meteorologist in Charge
Kwajalein Missile Range
PO Box 67
APO San Francisco, 96555

Director
NOAA/ERL/APCL R31
RB3-Room 567
Boulder, CO 80302

Library-R-51-Tech Reports
NOAA/ERL
320 S. Broadway
Boulder, CO 80302

National Center for Atmos Research
NCAR Library
PO Box 3000
Boulder, CO 80307

B. Girardo
Bureau of Reclamation
E&R Center, Code 1220
Denver Federal Center, Bldg 67
Denver, CO 80225

National Weather Service
National Meteorological Center
W321, WWB, Room 201
ATTN: Mr. Quiroz
Washington, DC 20233

Mil Assistant for Atmos Sciences
Ofc of the Undersecretary of Defense
for Rsch & Engr/E&LS - Room 3D129
The Pentagon
Washington, DC 20301

Defense Communications Agency
Technical Library Center
Code 205
Washington, DC 20305

Director
Defense Nuclear Agency
ATTN: Technical Library
Washington, DC 20305

HQDA (DAEN-RDM/Dr. de Percin)
Washington, DC 20314

Director
Naval Research Laboratory
Code 5530
Washington, DC 20375

Commanding Officer
Naval Research Laboratory
Code 2627
Washington, DC 20375

Dr. J. M. MacCallum
Naval Research Laboratory
Code 1409
Washington, DC 20375

The Library of Congress
ATTN: Exchange & Gift Div
Washington, DC 20540
2

Head, Atmos Rsch Section
Div Atmospheric Science
National Science Foundation
1800 G. Street, NW
Washington, DC 20550

CPT Hugh Albers, Exec Sec
Interdept Committee on Atmos Science
National Science Foundation
Washington, DC 20550

Director, Systems R&D Service
Federal Aviation Administration
ATTN: ARD-54
2100 Second Street, SW
Washington, DC 20590

ADTC/DLODL
Eglin AFB, FL 32542

Naval Training Equipment Center
ATTN: Technical Library
Orlando, FL 32813

Det 11, 2WS/OI
ATTN: Maj Orondorff
Patrick AFB, FL 32925

USAFETAC/CB
Scott AFB, IL 62225

HQ, ESD/TOSI/S-22
Hanscom AFB, MA 01731

Air Force Geophysics Laboratory
ATTN: LCB (A. S. Carten, Jr.)
Hanscom AFB, MA 01731

Air Force Geophysics Laboratory
ATTN: LYD
Hanscom AFB, MA 01731

Meteorology Division
AFGL/LY
Hanscom AFB, MA 01731

US Army Liaison Office
MIT-Lincoln Lab, Library A-032
PO Box 73
Lexington, MA 02173

Director
US Army Ballistic Rsch Lab
ATTN: DRDAR-BLB (Dr. G. E. Keller)
Aberdeen Proving Ground, MD 21005

Commander
US Army Ballistic Rsch Lab
ATTN: DRDAR-BLP
Aberdeen Proving Ground, MD 21005

Director
US Army Armament R&D Command
Chemical Systems Laboratory
ATTN: DRDAR-CLJ-I
Aberdeen Proving Ground, MD 21010

Chief CB Detection & Alarms Div
Chemical Systems Laboratory
ATTN: DRDAR-CLC-CR (H. Tannenbaum)
Aberdeen Proving Ground, MD 21010

Commander
Harry Diamond Laboratories
ATTN: DELHD-CO
2800 Powder Mill Road
Adelphi, MD 20783

Commander
ERADCOM
ATTN: DRDEL-AP
2800 Powder Mill Road
Adelphi, MD 20783
2

Commander
ERADCOM
ATTN: DRDEL-CG/DRDEL-DC/DRDEL-CS
2800 Powder Mill Road
Adelphi, MD 20783

Commander
ERADCOM
ATTN: DRDEL-CT
2800 Powder Mill Road
Adelphi, MD 20783

Commander
ERADCOM
ATTN: DRDEL-EA
2800 Powder Mill Road
Adelphi, MD 20783

Commander
ERADCOM
ATTN: DRDEL-PA/DRDEL-ILS/DRDEL-E
2800 Powder Mill Road
Adelphi, MD 20783

Commander
ERADCOM
ATTN: DRDEL-PAO (S. Kimmel)
2800 Powder Mill Road
Adelphi, MD 20783

Chief
Intelligence Materiel Dev & Support Ofc
ATTN: DELEW-WL-I
Bldg 4554
Fort George G. Meade, MD 20755

Acquisitions Section, IRDB-D823
Library & Info Service Div, NOAA
6009 Executive Blvd
Rockville, MD 20852

Naval Surface Weapons Center
White Oak Library
Silver Spring, MD 20910

The Environmental Research
Institute of MI
ATTN: IRIA Library
PO Box 8618
Ann Arbor, MI 48107

Mr. William A. Main
USDA Forest Service
1407 S. Harrison Road
East Lansing, MI 48823

Dr. A. D. Belmont
Research Division
PO Box 1249
Control Data Corp
Minneapolis, MN 55440

Director
Naval Oceanography & Meteorology
NSTL Station
Bay St Louis, MS 39529

Director
US Army Engr Waterways Experiment Sta
ATTN: Library
PO Box 631
Vicksburg, MS 39180

Environmental Protection Agency
Meteorology Laboratory
Research Triangle Park, NC 27711

US Army Research Office
ATTN: DRXRO-PP
PO Box 12211
Research Triangle Park, NC 27709

Commanding Officer
US Army Armament R&D Command
ATTN: DRDAR-TSS Bldg 59
Dover, NJ 07801

Commander
HQ, US Army Avionics R&D Activity
ATTN: DAVAA-O
Fort Monmouth, NJ 07703

Commander/Director
US Army Combat Surveillance & Target
Acquisition Laboratory
ATTN: DELCS-D
Fort Monmouth, NJ 07703

Commander
US Army Electronics R&D Command
ATTN: DELCS-S
Fort Monmouth, NJ 07703

Commander
US Army Electronics R&D Command
ATTN: DELCS-S (Dr. Swingle)
Fort Monmouth, NJ 07703
3

Director
US Army Electronics Technology &
Devices Laboratory
ATTN: DELET-D
Fort Monmouth, NJ 07703

Commander
US Army Electronic Warfare Laboratory
ATTN: DELEW-D
Fort Monmouth, NJ 07703

Commander
US Army Night Vision &
Electro-Optics Laboratory
ATTN: DELNV-L (Dr. Rudolf Buser)
Fort Monmouth, NJ 07703

Commander
ERADCOM Technical Support Activity
ATTN: DELSD-L
Fort Monmouth, NJ 07703

Project Manager, FIREFINDER
ATTN: DRCPM-FF
Fort Monmouth, NJ 07703

Project Manager, REMBASS
ATTN: DRCPM-RBS
Fort Monmouth, NJ 07703

Commander
US Army Satellite Comm Agency
ATTN: DRCPM-SC-3
Fort Monmouth, NJ 07703

Commander
ERADCOM Scientific Advisor
ATTN: DRDEL-SA
Fort Monmouth, NJ 07703

6585 TG/WE
Holloman AFB, NM 88330

AFWL/WE
Kirtland, AFB, NM 87117

AFWL/Technical Library (SUL)
Kirtland AFB, NM 87117

Commander
US Army Test & Evaluation Command
ATTN: STEWS-AD-L
White Sands Missile Range, NM 88002

Rome Air Development Center
ATTN: Documents Library
TSLD (Bette Smith)
Griffiss AFB, NY 13441

Commander
US Army Tropic Test Center
ATTN: STETC-TD (Info Center)
APO New York 09827

Commandant
US Army Field Artillery School
ATTN: ATSF-CD-R (Mr. Farmer)
Fort Sill, OK 73503

Commandant
US Army Field Artillery School
ATTN: ATSF-CF-R
Fort Sill, OK 73503

Director CFD
US Army Field Artillery School
ATTN: Met Division
Fort Sill, OK 73503

Commandant
US Army Field Artillery School
ATTN: Morris Swett Library
Fort Sill, OK 73503

Commander
US Army Dugway Proving Ground
ATTN: MT-DA-L
Dugway, UT 84022

William Peterson
Research Associates
Utah State University, UNC 48
Logan, UT 84322

Inge Dirmhirn, Professor
Utah State University, UNC 48
Logan, UT 84322

Defense Documentation Center
ATTN: DDC-TCA
Cameron Station, Bldg 5
Alexandria, VA 22314
12

Commanding Officer
US Army Foreign Sci & Tech Center
ATTN: DRXST-IS1
220 7th Street, NE
Charlottesville, VA 22901

Naval Surface Weapons Center
Code G65
Dahlgren, VA 22448

Commander
US Army Night Vision
& Electro-Optics Lab
ATTN: DELNV-D
Fort Belvoir, VA 22060

Commander and Director
US Army Engineer Topographic Lab
ETL-TD-MB
Fort Belvoir, VA 22060

Director
Applied Technology Lab
DAVDL-EU-TSD
ATTN: Technical Library
Fort Eustis, VA 23604

Department of the Air Force
OL-C, 5WW
Fort Monroe, VA 23651

Department of the Air Force
5WW/DN
Langley AFB, VA 23665

Director
Development Center MCDEC
ATTN: Firepower Division
Quantico, VA 22134

US Army Nuclear & Chemical Agency
ATTN: MONA-WE
Springfield, VA 22150

Director
US Army Signals Warfare Laboratory
ATTN: DELSW-OS (Dr. R. Burkhardt)
Vint Hill Farms Station
Warrenton, VA 22186

Commander
US Army Cold Regions Test Center
ATTN: STECR-OP-PM
APO Seattle, 98733

US Army Materiel Systems
  Analysis Activity
ATTN: DRXSY-MP
Aberdeen Proving Ground, MD 21005

ATMOSPHERIC SCIENCES RESEARCH PAPERS

1. Lindberg, J.D., "An Improvement to a Method for Measuring the Absorption Coefficient of Atmospheric Dust and other Strongly Absorbing Powders, " ECOM-5565, July 1975.
2. Avara, Elton, P., "Mesoscale Wind Shears Derived from Thermal Winds," ECOM-5566, July 1975.
3. Gomez, Richard B., and Joseph H. Pierluissi, "Incomplete Gamma Function Approximation for King's Strong-Line Transmittance Model," ECOM-5567, July 1975.
4. Blanco, A.J., and B.F. Engebos, "Ballistic Wind Weighting Functions for Tank Projectiles," ECOM-5568, August 1975.
5. Taylor, Fredrick J., Jack Smith, and Thomas H. Pries, "Crosswind Measurements through Pattern Recognition Techniques," ECOM-5569, July 1975.
6. Walters, D.L., "Crosswind Weighting Functions for Direct-Fire Projectiles," ECOM-5570, August 1975.
7. Duncan, Louis D., "An Improved Algorithm for the Iterated Minimal Information Solution for Remote Sounding of Temperature," ECOM-5571, August 1975.
8. Robbiani, Raymond L., "Tactical Field Demonstration of Mobile Weather Radar Set AN/TPS-41 at Fort Rucker, Alabama," ECOM-5572, August 1975.
9. Miers, B., G. Blackman, D. Langer, and N. Lorimier, "Analysis of SMS/GOES Film Data," ECOM-5573, September 1975.
10. Manquero, Carlos, Louis Duncan, and Rufus Bruce, "An Indication from Satellite Measurements of Atmospheric CO2 Variability," ECOM-5574, September 1975.
11. Petracca, Carmine, and James D. Lindberg, "Installation and Operation of an Atmospheric Particulate Collector," ECOM-5575, September 1975.
12. Avara, Elton P., and George Alexander, "Empirical Investigation of Three Iterative Methods for Inverting the Radiative Transfer Equation," ECOM-5576, October 1975.
13. Alexander, George D., "A Digital Data Acquisition Interface for the SMS Direct Readout Ground Station — Concept and Preliminary Design," ECOM-5577, October 1975.
14. Cantor, Israel, "Enhancement of Point Source Thermal Radiation Under Clouds in a Nonattenuating Medium," ECOM-5578, October 1975.
15. Norton, Colburn, and Glenn Hoidale, "The Diurnal Variation of Mixing Height by Month over White Sands Missile Range, N.M," ECOM-5579, November 1975.
16. Avara, Elton P., "On the Spectrum Analysis of Binary Data," ECOM-5580, November 1975.
17. Taylor, Fredrick J., Thomas H. Pries, and Chao-Huan Huang, "Optimal Wind Velocity Estimation," ECOM-5581, December 1975.
18. Avara, Elton P., "Some Effects of Autocorrelated and Cross-Correlated Noise on the Analysis of Variance, " ECOM-5582, December 1975.
19. Gillespie, Patti S., R.L. Armstrong, and Kenneth O. White, "The Spectral Characteristics and Atmospheric CO2 Absorption of the Ho^{+3}:YLF Laser at 2.05μm," ECOM-5583, December 1975.
20. Novlan, David J. "An Empirical Method of Forecasting Thunderstorms for the White Sands Missile Range," ECOM-5584, February 1976.
21. Avara, Elton P., "Randomization Effects in Hypothesis Testing with Autocorrelated Noise," ECOM-5585, February 1976.
22. Watkins, Wendell R., "Improvements in Long Path Absorption Cell Measurement," ECOM-5586, March 1976.
23. Thomas, Joe, George D. Alexander, and Marvin Dubbin, "SATTEL — An Army Dedicated Meteorological Telemetry System," ECOM-5587. March 1976.
24. Kennedy, Bruce W., and Delbert Bynum, "Army User Test Program for the RDT&E-XM-75 Meteorological Rocket," ECOM-5588, April 1976.

25. Barnett, Kenneth M., ' A Description of the Artillery Meteorological Comparisons at White Sands Missle Range, October 1974 - December 1974 ('PASS' - Prototype Artillery [Meteorological] Subsystem)," ECOM-5589, April 1976.
26. Miller, Walter B., "Preliminary Analysis of Fall-of-Shot From Project 'PASS'," ECOM-5590, April 1976.
27. Avara, Elton P., "Error Analysis of Minimum Information and Smith's Direct Methods for Inverting the Radiative Transfer Equation," ECOM-5591, April 1976.
28. Yee, Young P., James D. Horn, and George Alexander, "Synoptic Thermal Wind Calculations from Radiosonde Observations Over the Southwestern United States," ECOM-5592, May 1976.
29. Duncan, Louis D., and Mary Ann Seagraves, "Applications of Empirical Corrections to NOAA-4 VTPR Observations," ECOM-5593, May 1976.
30. Miers, Bruce T., and Steve Weaver, "Applications of Meterological Satellite Data to Weather Sensitive Army Operations,"ECOM-5594, May 1976.
31. Sharenow, Moses, "Redesign and Improvement of Balloon ML-566," ECOM-5595, June, 1976.
32. Hansen, Frank V., "The Depth of the Surface Boundary Layer," ECOM-5596, June 1976.
33. Pinnick, R.G., and E.B. Stenmark, "Response Calculations for a Commercial Light-Scattering Aerosol Counter," ECOM-5597, July 1976.
34. Mason, J., and G.B. Hoidale, "Visibility as an Estimator of Infrared Transmittance," ECOM-5598, July 1976.
35. Bruce, Rufus E., Louis D. Duncan, and Joseph H. Pierluissi, "Experimental Study of the Relationship Between Radiosonde Temperatures and Radiometric-Area Temperatures," ECOM-5599, August 1976.
36. Duncan, Louis D., "Stratospheric Wind Shear Computed from Satellite Thermal Sounder Measurements," ECOM-5800, September 1976.
37. Taylor, F., P. Mohan, P. Joseph and T. Pries, "An All Digital Automated Wind Measurement System," ECOM-5801, September 1976.
38. Bruce, Charles, "Development of Spectrophones for CW and Pulsed Radiation Sources," ECOM-5802, September 1976.
39. Duncan, Louis D., and Mary Ann Seagraves,"Another Method for Estimating Clear Column Radiances," ECOM-5803, October 1976.
40. Blanco, Abel J., and Larry E. Taylor, "Artillery Meteorological Analysis of Project Pass," ECOM-5804, October 1976.
41. Miller, Walter, and Bernard Engebos," A Mathematical Structure for Refinement of Sound Ranging Estimates," ECOM-5805, November, 1976.
42. Gillespie, James B., and James D. Lindberg, "A Method to Obtain Diffuse Reflectance Measurements from 1.0 to 3.0 μm Using a Cary 171 Spectrophotometer," ECOM-5806, November 1976.
43. Rubio, Roberto, and Robert O. Olsen,"A Study of the Effects of Temperature Variations on Radio Wave Absorption,"ECOM-5807, November 1976.
44. Ballard, Harold N., "Temperature Measurements in the Stratosphere from Balloon-Borne Instrument Platforms, 1968-1975," ECOM-5808, December 1976.
45. Monahan, H.H., "An Approach to the Short-Range Prediction of Early Morning Radiation Fog," ECOM-5809, January 1977.
46. Engebos, Bernard Francis, "Introduction to Multiple State Multiple Action Decision Theory and Its Relation to Mixing Structures," ECOM-5810, January 1977.
47. Low, Richard D.H.,"Effects of Cloud Particles on Remote Sensing from Space in the 10-Micrometer Infrared Region," ECOM-5811, January 1977.
48. Bonner, Robert S., and R. Newton, "Application of the AN/GVS-5 Laser Rangefinder to Cloud Base Height Measurements," ECOM-5812, February 1977.
49. Rubio, Roberto, "Lidar Detection of Subvisible Reentry Vehicle Erosive Atmospheric Material," ECOM-5813, March 1977.
50. Low, Richard D.H., and J.D. Horn, "Mesoscale Determination of Cloud-Top Height: Problems and Solutions," ECOM-5814, March 1977.

51. Duncan, Louis D., and Mary Ann Seagraves, "Evaluation of the NOAA-4 VTPR Thermal Winds for Nuclear Fallout Predictions," ECOM-5815, March 1977.
52. Randhawa, Jagir S., M. Izquierdo, Carlos McDonald and Zvi Salpeter, "Stratospheric Ozone Density as Measured by a Chemiluminescent Sensor During the Stratcom VI-A Flight," ECOM-5816, April 1977.
53. Rubio, Roberto, and Mike Izquierdo, "Measurements of Net Atmospheric Irradiance in the 0.7- to 2.8-Micrometer Infrared Region," ECOM-5817, May 1977.
54. Ballard, Harold N., Jose M. Serna, and Frank P. Hudson Consultant for Chemical Kinetics, "Calculation of Selected Atmospheric Composition Parameters for the Mid-Latitude, September Stratosphere," ECOM-5818, May 1977.
55. Mitchell, J.D., R.S. Sagar, and R.O. Olsen, "Positive Ions in the Middle Atmosphere During Sunrise Conditions," ECOM-5819, May 1977.
56. White, Kenneth O., Wendell R. Watkins, Stuart A. Schleusener, and Ronald L. Johnson, "Solid-State Laser Wavelength Identification Using a Reference Absorber," ECOM-5820, June 1977.
57. Watkins, Wendell R., and Richard G. Dixon, "Automation of Long-Path Absorption Cell Measurements," ECOM-5821, June 1977.
58. Taylor, S.E., J.M. Davis, and J.B. Mason, "Analysis of Observed Soil Skin Moisture Effects on Reflectance," ECOM-5822, June 1977.
59. Duncan, Louis D. and Mary Ann Seagraves, "Fallout Predictions Computed from Satellite Derived Winds," ECOM-5823. June 1977.
60. Snider, D.E., D.G. Murcray, F.H. Murcray, and W.J. Williams, "Investigation of High-Altitude Enhanced Infrared Backround Emissions" (U), SECRET, ECOM-5824, June 1977.
61. Dubbin, Marvin H. and Dennis Hall, "Synchronous Meteorlogical Satellite Direct Readout Ground System Digital Video Electronics," ECOM-5825, June 1977.
62. Miller, W., and B. Engebos, "A Preliminary Analysis of Two Sound Ranging Algorithms," ECOM-5826, July 1977.
63. Kennedy, Bruce W., and James K. Luers, "Ballistic Sphere Techniques for Measuring Atomspheric Parameters," ECOM-5827, July 1977.
64. Duncan, Louis D., "Zenith Angle Variation of Satellite Thermal Sounder Measurements," ECOM-5828, August 1977.
65. Hansen, Frank V., "The Critical Richardson Number," ECOM-5829, September 1977.
66. Ballard, Harold N., and Frank P. Hudson (Compilers), "Stratospheric Composition Balloon-Borne Experiment," ECOM-5830, October 1977.
67. Barr, William C., and Arnold C. Peterson, "Wind Measuring Accuracy Test of Meteorological Systems," ECOM-5831, November 1977.
68. Ethridge, G.A. and F.V. Hansen, "Atmospheric Diffusion: Similarity Theory and Empirical Derivations for Use in Boundary Layer Diffusion Problems," ECOM-5832, November 1977.
69. Low, Richard D.H., "The Internal Cloud Radiation Field and a Technique for Determining Cloud Blackness," ECOM-5833, December 1977.
70. Watkins, Wendell R., Kenneth O. White, Charles W. Bruce, Donald L. Walters, and James D. Lindberg, "Measurements Required for Prediction of High Energy Laser Transmission," ECOM-5834, December 1977.
71. Rubio, Robert, "Investigation of Abrupt Decreases in Atmospherically Backscattered Laser Energy," ECOM-5835. December 1977.
72. Monahan, H.H. and R.M. Cionco, "An Interpretative Review of Existing Capabilities for Measuring and Forecasting Selected Weather Variables (Emphasizing Remote Means)," ASL-TR-0001, January 1978.
73. Heaps. Melvin G., "The 1979 Solar Eclipse and Validation of D-Region Models," ASL-TR-0002. March 1978.

74. Jennings, S.G., and J.B. Gillespie, "M.I.E. Theory Sensitivity Studies - The Effects of Aerosol Complex Refractive Index and Size Distribution Variations on Extinction and Absorption Coefficients Part II: Analysis of the Computational Results," ASL-TR-0003, March 1978.

75. White, Kenneth O. et al, "Water Vapor Continuum Absorption in the 3.5µm to 4.0µm Region," ASL-TR-0004, March 1978.

76. Olsen, Robert O., and Bruce W. Kennedy, "ABRES Pretest Atmospheric Measurements," ASL-TR-0005, April 1978.

77. Ballard, Harold N., Jose M. Serna, and Frank P. Hudson, "Calculation of Atmospheric Composition in the High Latitude September Stratosphere," ASL-TR-0006, May 1978.

78. Watkins, Wendell R. et al, "Water Vapor Absorption Coefficients at HF Laser Wavelengths," ASL-TR-0007, May 1978.

79. Hansen, Frank V., "The Growth and Prediction of Nocturnal Inversions," ASL-TR-0008, May 1978.

80. Samuel, Christine, Charles Bruce, and Ralph Brewer, "Spectrophone Analysis of Gas Samples Obtained at Field Site," ASL-TR-0009, June 1978.

81. Pinnick, R.G. et al., "Vertical Structure in Atmospheric Fog and Haze and its Effects on IR Extinction," ASL-TR-0010, July 1978.

82. Low, Richard D.H., Louis D. Duncan, and Richard B. Gomez, "The Microphysical Basis of Fog Optical Characterization," ASL-TR-0011, August 1978.

83. Heaps, Melvin G., "The Effect of a Solar Proton Event on the Minor Neutral Constituents of the Summer Polar Mesosphere," ASL-TR-0012, August 1978.

☆ U.S. GOVERNMENT PRINTING OFFICE: 1978 777-093/ 13